ELSEVIER

publ.
1. Februar 1998

Solid State Ionics 106 (1998) 263–268

SOLID STATE IONICS

Sintering behaviors of ceria and gadolinia-doped ceria

Hideaki Inaba[a,*], Toshifumi Nakajima[b], Hiroaki Tagawa[b]

[a]*Technical Research Laboratories, Kawasaki Steel Corporation, Kawasaki Chou, Chuo-ku, Chiba 260, Japan*
[b]*Institute of Environmental Science and Technology Research Center, Yokohama National University, 154 Tokiwadai, Hodogaya-ku, Yokohama 240, Japan*

Received 5 January 1997; accepted 6 September 1997

Abstract

Sintering behaviors of ceria powders with large and fine particle size and gadolinia-doped ceria powders with a fine particle size have been studied by measuring density and grain size as a function of sintering time. Densification rate and grain growth rate of ceria with a fine particle size were larger than those with a large particle size. Grain growth rate of gadolinia-doped ceria was much smaller than that of ceria, while densification rate was considerably larger. Inhibition of grain growth observed in gadolinia-doped ceria was explained by the solute drag model due to a space charge effect. The fact that the densification rate in gadolinia-doped ceria was considerably larger than that in ceria suggests that the rate determining step of densification is the diffusion of oxygen. In gadolinia-doped ceria, the diffusion of oxygen is larger, the shrinkage of internal pores is considered to proceed faster due to larger mobility of oxygen and then the densification rate becomes larger than in ceria.

Keywords: Ceria; Doped ceria; Sintering; Densification; Grain growth

1. Introduction

Solid electrolytes have received increasing attention in recent years due to their excellent suitability as ionically conductive materials in high temperature systems. For the applications requiring ionic conduction, such as solid oxide fuel cells or oxygen sensors, the fluorite oxides have been extensively investigated [1–4]. Among them, yttria-stabilized zirconia with the cubic fluorite structure has been most extensively investigated and practically used. Although yttria-stabilized zirconia is the most reliable candidate as the electrolyte for the solid oxide fuel cells so far, its electrical conductivity is not high enough and it requires a high operating temperature such as 1273 K. The alternative solid electrolyte for yttria-stabilized zirconia has been studied, which should possess a higher electric conductivity than that of yttria-stabilized zirconia and for operation at lower temperatures such as 1073 K. Thus gadolinia-doped ceria electrolytes have been given much attention as an alternative of the yttria-stabilized zirconia as the electrolyte in solid oxide fuel cells [4].

In the application of ceria-based electrolytes for solid oxide fuel cells, sintering of these oxides is important in order to obtain dense sintered materials. Sintering of the zirconia-based oxides has been

*Corresponding author. Guest Professor of the Institute of Environmental Science and Technology Research Center, Yokohama National University. Present address: Faculty of Education, Chiba University, 1-33 Yayoi-Chou, Inage-ku, Chiba 263, Japan.

PII S0167-2738(97)00496-7

studied by many investigators [5–9] and the solute effect of dopants is shown to have an important role in the sintering process. Recently, sintering behavior of yttria-doped ceria was studied by Upadhyaya et al. [10] showing the importance of the solute effect, but no kinetic data on grain growth and densification were given.

In the present study, the sintering behaviors of ceria and gadolinia-doped ceria were studied by observing the change of density and grain size as a function of temperature and time. The effect of particle size of raw materials for ceria and the effect of gadolinia doping on grain growth rate and densification rate were examined and discussed.

2. Experimental

Starting materials were ceria with average particle size of 0.07 μm (sample A) and 0.02 μm (sample B) and 20 mol% gadolinia-doped ceria ($Ce_{0.8}Gd_{0.2}O_{1.9}$, sample C) with average particle size of 0.03 μm. Sample A with a purity of 99.9% was provided by Rare Metallic Co., Ltd. Sample B and C with a purity of 99.9% were provided by Anan Kasei Co., Ltd. The average particle size was determined by using a transmission electron microscope (TEM). Cylindrical pellets 7 mm in diameter and about 3 mm in height were obtained by pressing the powders at about 150 MPa. Linear shrinkage along an axial direction during sintering was measured in air at a heating rate of 5 K min^{-1} by using a dilatometer of push-rod type made by Rigaku Denki Co., Ltd. The pressed sample pellets were sintered in air at 1273, 1473 and 1673 K for 1, 3 and 7 h. The densities of sintered samples were obtained from the measurements of mass and volume of the pellets. The microstructure of the sintered samples was observed by using a scanning electron microscope (SEM).

* 1000, 1200 and 1400°C

3. Results

The TEM photographs of samples A, B and C are shown in Fig. 1. The average particle diameters of samples A, B and C were determined from the photographs as 0.07, 0.02 and 0.03 μm, respectively. The average particle diameter of sample B was considerably smaller than that of sample A and can be regarded as essentially the same as sample C.

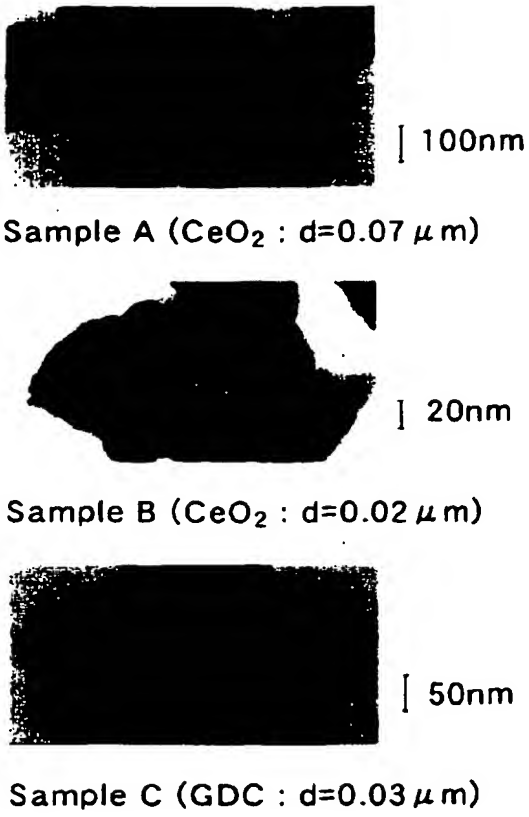

Fig. 1. TEM photographs for samples A, B and C.

Using the pressed pellets, linear shrinkage during sintering was measured by the dilatometer for samples A, B and C and the results are shown in Fig. 2 as a function of temperature. It is seen from Fig. 2 that sample B shrinks faster than sample A. This is due to a larger surface reactivity in sample B resulting from the finer average particle size. Sample C also had a fine average particle size and showed a fast linear shrinkage especially at lower temperatures, but the shrinkage became smaller compared with sample B at high temperatures. This smaller shrinkage at high temperatures is considered to be originated from inhibition of grain growth due to the presence of dopant, as will be discussed later.

The densities of the samples A, B and C as a function of sintering time at 1473 and 1673 K are

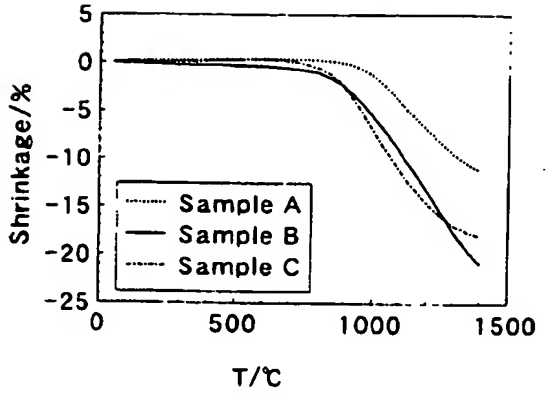

Fig. 2. Linear shrinkage for samples A, B and C during sintering as a function of temperature.

shown in Figs. 3 and 4, respectively. These figures show that logarithm of the density is linearly dependent on that of the sintering time. Densification rate of sample B was larger than sample A. This is due also to a larger surface reactivity in sample B resulting from the finer average particle size. Densification rate of sample C was larger than sample B. Since the average particle size of sample C is nearly the same as sample B, this effect is due to the difference in the chemical composition.

An example of SEM photographs for samples after sintering is shown in Fig. 5. The grain size of

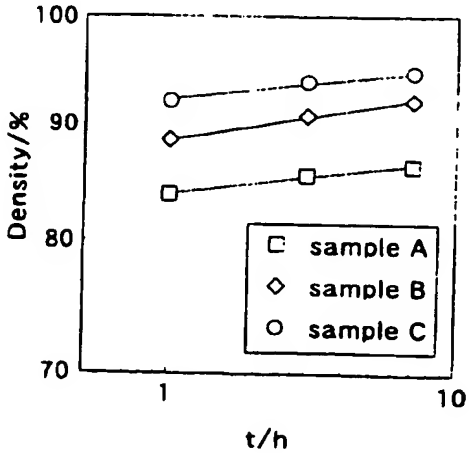

Fig. 3. Density of the samples A, B and C as a function of sintering time at 1473 K.

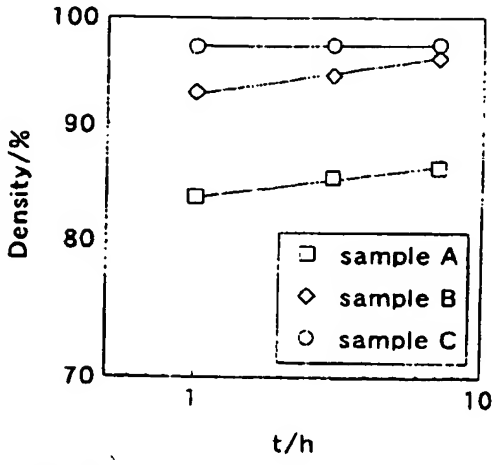

Fig. 4. Density of the samples A, B and C as a function of sintering time at 1673 K.

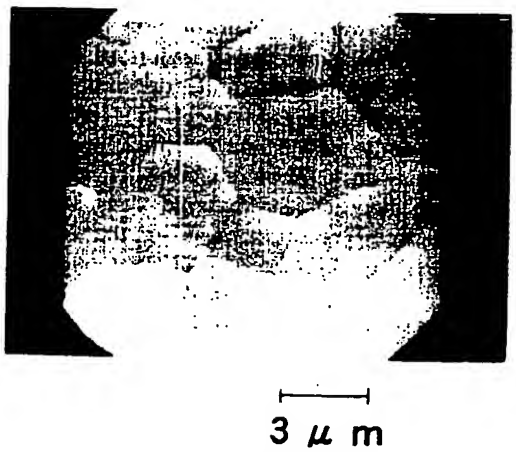

Fig. 5. An example of SEM photographs for the sintered specimen.

sintered samples was determined from the SEM image by approximating each grain as a square. The grain sizes thus determined for samples A, B and C after sintering at 1673 K are shown in Fig. 6 as a function of sintering time. The grain size of sample B is originally small but becomes larger during the course of sintering as compared with sample A, while the grain size of sample C is originally small and remains small as compared with samples A and B.

It would be convenient to use a parameter describ-

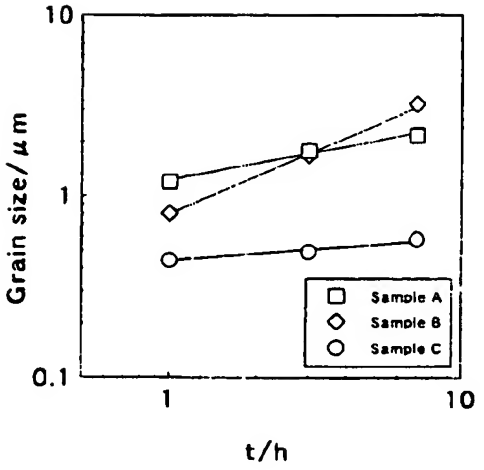

Fig. 6. Grain sizes for samples A, B and C after sintering at 1673 K as a function of reaction time.

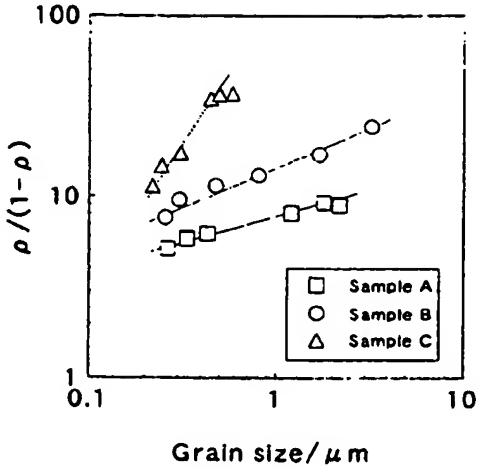

Fig. 7. The relation between the relative density ρ and average particle/grain size d according to Eq. (1).

ing the ratio between the densification rate and the grain growth rate, since the behaviors of densification and grain growth are quite different between samples B and C. Ikegami et al. [11] proposed a model that grain growth and densification progress simultaneously in a powdered compact, expressing the relation between the relative density ρ and average particle/grain size d using the following equation:

$$\log\rho(1-\rho_0)/\rho_0(1-\rho) = K\log(d/d_0). \quad (1)$$

where ρ_0 is the initial particle size, d_0 is the green density and K is a constant depending on the spread of the distribution of particle/grain size and surface area of pore and particle/grain. The relation between the relative density ρ and average particle/grain size d according to Eq. (1) is shown in Fig. 7. Linear relationships hold for all the samples as seen in Fig. 7. Since the proportional constant K can be regarded as a parameter showing the relative densification rate/grain growth rate ratio, sample C has the largest densification rate/grain growth rate ratio as shown in Fig. 7.

The pore size distributions for samples A, B and C were obtained from the SEM photographs of fractured surface after sintering for 7 h at 1673 K and are shown in Fig. 8. The pore size distribution becomes narrower when the original particle size is finer as compared between samples A and B and it is narrowest in sample C as seen in Fig. 8.

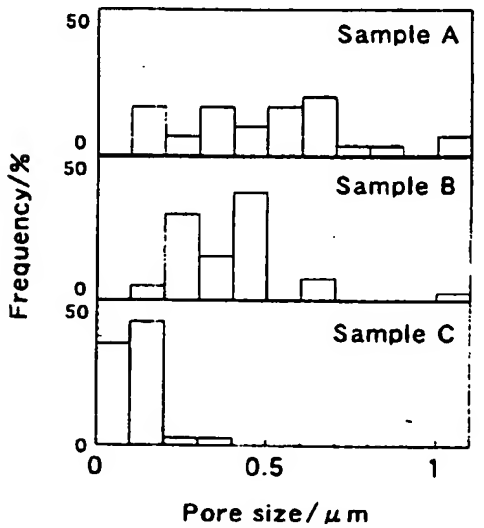

Fig. 8. Pore size distributions for samples A, B and C obtained from the SEM photographs of fractured surface.

4. Discussion

The difference of sintering behavior between

samples A and B originates from the difference of particle size, since the chemical composition of both samples is the same. Sample B with a smaller particle size has a larger surface energy and gives a larger densification rate and a grain growth rate and the relative densification rate/grain growth rate ratio than sample A as seen in Figs. 3, 4, 6 and 7. In the sample with a smaller particle/grain size, diffusion near the surface/grain boundary during sintering may be faster and it would contribute to both densification and grain growth [12–14]. Zhao and Harmer [15] proposed a model on the effect of pore size distribution at the final stage of sintering and predicted that increasing the number of pores per grain increased densification rate, grain growth rate, and the ratio of relative densification rate/grain growth. Since the grain size of sample B is larger than sample A at the final stage of sintering as seen in Fig. 6 and pore size distribution is narrower than sample A as seen in Fig. 8, the number of pores per grain of sample B is larger than sample A. Larger densification rate, grain growth rate, and the relative densification rate/grain growth rate ratio of sample B are thus obtained as Zhao and Harmer [15] predicted.

The difference of sintering behavior between samples B and C originates from the difference of the chemical composition: ceria and gadolinia-doped ceria, respectively, since particle sizes of both samples are nearly the same. As seen in Figs. 3, 4 and 6, sample C shows the larger densification rate, but much smaller grain growth rate than sample B. This sintering behavior of sample C is well characterized by the largest K in Eq. (1) among the samples as seen in Fig. 7 showing the largest densification rate/grain growth rate ratio. The fact that sample C showed large densification rate but much smaller grain growth rate would indicate that the mechanisms of densification and grain growth are different in these samples.

As seen in Fig. 6, addition of gadolinia to ceria decreases the grain growth rate. This inhibiting behavior of dopant in grain growth may be the same as was observed in MgO-doped Al_2O_3, $CaCl_2$-doped KCl, and ThO_2-doped Y_2O_3 which was explained by the solute drag model due to a space charge effect [16]. Inhibition in grain growth was also observed in doped zirconia [8,9] and yttria-doped ceria [10] and explained by the same mechanism. When a tri-valent dopant with an effective negative charge is present in the bulk of grain, the charge neutrality is attained by creating oxygen vacancies. The oxygen vacancies would concentrate and create effective positive charge in the surface/grain boundary due to surface/grain energy. The dopant segregates to the region adjacent to the surface/grain boundary by Coulomb attraction of the space charge. This implies the presence of an enrichment layer of dopants at the grain boundaries. Excess dopant localized at the boundaries generates a steep gradient between bulk and intergrain interfaces. Thus, the dopant (solute) gradient gives a strong drag to the grain boundary mobility, resulting in an inhibition of grain growth. Direct experimental evidence for such a solute enrichment in grain boundary has been obtained by various electronic optical techniques [9,17,18]. In yttria-doped ceria [10], grain growth rate is reported to be decreased as the yttria content is increased. Therefore, a much slower grain growth rate observed in gadolinia-doped ceria is considered to be due to the solute drag.

The dependence of dopant concentration on densification rate seems not to be clear in doped zirconia [8,9] and yttria-doped ceria [10]. It is seen, however, in Figs. 3 and 4 that the densification rate in sample C is larger than that of sample B, although the grain growth rate in sample C is much smaller. This fact indicates that densification and grain growth have different mechanisms between samples B and C. Since densification is attained by shrinkage and/or removal of pores and by releasing oxygen gas from pores, the transport of oxygen would be a rate determining step in densification. The diffusion rate of oxygen in the bulk would be a rate determining step in densification, since the oxygen partial pressure in pores is considered to be limited by the diffusion of oxygen in the bulk. Similar effect of oxygen partial pressure on the sintering process was studied in Mn–Zn ferrites by Inaba [19]. Oxygen diffusion in a fluorite structure was reviewed by Inaba and Tagawa [4] and oxygen diffusion in gadolinia-doped ceria is suggested to be faster than that of ceria using the experimental data on diffusion of ceria by Floyd [20] and electrical conductivity of gadolinia-doped ceria. Thus we can understand that the larger densification rate in gadolinia-doped ceria originates from the larger mobility of oxygen.

5. Conclusions

Sintering behaviors of ceria of samples with a large and fine particle size and gadolinia-doped ceria sample with a fine particle size were studied by measuring density and grain size as a function of sintering time.

1. Densification rate and grain growth rate in a sample with a fine particle size were larger than those with a large particle size resulting from the larger surface energy in a fine powder sample.
2. Grain growth rate of gadolinia-doped ceria was much smaller than that of ceria. Inhibition in grain growth observed in gadolinia-doped ceria was explained by the solute drag effect due to a space charge.
3. Densification rate of gadolinia-doped ceria was considerably larger than that of ceria, although grain growth rate was much smaller. Densification was considered to be determined mainly by diffusion of oxygen, since the rate of shrinkage and/or removal of pores may be limited by diffusion of oxygen. The larger densification rate in gadolinia-doped ceria was considered to originate from the larger mobility of oxygen.

Acknowledgements

The authors wish to thank Anan Kasei Co., Ltd. for providing fine ceria and gadolinia-doped ceria powders.

References

[1] B.C.H. Steele, in: T. Takahashi (Ed.), High Conductivity Solid Ionic Conductors, World Scientific, Singapore, 1989.
[2] J.A. Kilner, B.C.H. Steele, in: O.T. Sorensen (Ed.), Non-stoichiometric Oxides, Academic Press, New York, 1981.
[3] R.M. Dell, A. Hooper, in: P. Hagenmuller, W. Van Gool, (Eds.), Solid Electrolytes, Academic Press, New York, 1978, p. 291.
[4] H. Inaba, H. Tagawa, Solid State Ionics 83 (1996) 1.
[5] M.E.S. Ali, O.T. Sorensen, S. Meriani, Sci. Ceram. 12 (1984) 355.
[6] A.J.A. Winnubst, G.S.A.M. Theunissen, W.F.M.G. Zervert, A.J. Berggraaf, Sci. Ceram. 14 (1988) 309.
[7] N.M. Ghoniem, S.B. Hanna, J. Mater. Sci. 25 (1990) 5192.
[8] S. Hwang, I. Chen, J. Am. Ceram. Soc. 73 (1990) 3269.
[9] M.M.R. Boutz, A.J.A. Winnubst, A.J. Berggraaf, J. Eur. Ceram. Soc. 13 (1994) 89.
[10] D.D. Upadhyaya, R. Bhat, S. Ramanathan, S.K. Roy, H. Schubert, G. Petzow, J. Eur. Ceram. Soc. 14 (1994) 337.
[11] T. Ikegami, M. Tsutsumi, S. Matsuda, S. Shirasaki, H. Suzuki, J. Appl. Phys. 49 (1978) 4238.
[12] G.C. Kuczynski, Trans. AIME 185 (1949) 169.
[13] R.L. Coble, J. Appl. Phys. 32 (1961) 787.
[14] R.L. Coble, J. Appl. Phys. 32 (1961) 793.
[15] J. Zhao, M.P. Harmer, J. Am. Ceram. Soc. 71 (1988) 113.
[16] W.D. Kingery, H.K. Bowen, D.R. Uhlmann, Introduction to Ceramics, 2nd ed., John Wiley, New York, 1976, p. 456.
[17] M.M.R. Boutz, C.S. Chen, L. Winnubst, A.J. Berggraaf, J. Am. Ceram Soc. 77 (1994) 2632.
[18] G.S.A.M. Theunissen, A.J.A. Winnubst, A.J. Berggraaf, J. Mater. Sci. 27 (1992) 5057.
[19] H. Inaba, Proceedings of 1993 Powder Metallurgy World Congress, Kyoto, 1993, p. 381.
[20] J.M. Floyd, Ind. J. Technol. 11 (1973) 589.